Title

Near-Infrared Dye-Labeled Anti-Prostate Stem Cell Antigen Minibody Enables Real-Time Fluorescence Imaging and Targeted Surgery in Translational Mouse Models

Journal

Clinical Cancer Research, 25(1)

ISSN

1078-0432

Authors

Zhang, Mo
Kobayashi, Naoko
Zettlitz, Kirstin A
et al.

Publication Date

2019

DOI

10.1158/1078-0432.ccr-18-1382

Peer reviewed

HHS Public Access

Author manuscript

Clin Cancer Res. Author manuscript; available in PMC 2020 January 01.

Published in final edited form as:

Clin Cancer Res. 2019 January 01; 25(1): 188–200. doi:10.1158/1078-0432.CCR-18-1382.

Near-infrared-dye labeled anti-Prostate Stem Cell Antigen minibody enables real-time fluorescence imaging and targeted surgery in translational mouse models

Mo Zhang[1,2], **Naoko Kobayashi**[1], **Kirstin A. Zettlitz**[3], **Evelyn A. Kono**[1], **Joyce Yamashiro**[1], **Wen-Ting K. Tsai**[3], **Ziyue K. Jiang**[1], **Chau P. Tran**[1], **Chung Wang**[1], **Johnny Guan**[1], **Anna M. Wu**[3], and **Robert E. Reiter**[1,*]

[1]Department of Urology, David Geffen School of Medicine, University of California Los Angeles, California, USA

[2]Department of Urology, Shengjing Hospital, China Medical University, Shenyang, China

[3]Crump Institute for Molecular Imaging, Department of Molecular and Medical Pharmacology, University of California Los Angeles, California, USA

Abstract

Purpose: The inability to intraoperatively distinguish the primary tumor, as well as lymphatic spread, increases the probability of positive surgical margins, tumor recurrence, and surgical toxicity. The goal of this study was to develop a tumor-specific optical probe for real-time fluorescence-guided surgery.

Experimental design: A humanized antibody fragment against PSCA (A11 minibody, A11 Mb) was conjugated with a near-infrared fluorophore, IRDye800CW. The integrity and binding of the probe to PSCA were confirmed by gel electrophoresis, size exclusion chromatography, and flow cytometry, respectively. The ability of the probe to detect tumor infiltrated lymph nodes and metastatic lesions was evaluated in two xenograft models, and in transgenic mice expressing human PSCA (hPSCA). An invasive intramuscular model was utilized to evaluate the efficacy of the A11 Mb-IRDye800CW-guided surgery.

[*]**Correspondence**: Robert E. Reiter, M.D., M.B.A., Department of Urology, David Geffen School of Medicine at UCLA, Box 951738, Los Angeles, CA 90095-1738, Phone number: 1 (310) 794-7224, rreiter@mednet.ucla.edu.

Authors' Contributions

Conception and design: M. Zhang, N. Kobayashi, K.A. Zettlitz, Z. K. Jiang, A.M. Wu, R.E. Reiter.

Development of methodology: M. Zhang, N. Kobayashi, K.A. Zettlitz, W.K. Tsai, Z. K. Jiang, E.A. Kono, A.M. Wu, R.E. Reiter.

Acquisition of data (provided animals, acquired and managed patients, provided facilities, etc.): M. Zhang, N. Kobayashi, E.A. Kono, J. Yamashiro, W.K. Tsai, K.A. Zettlitz,

Analysis and interpretation of data (e.g., statistical analysis, biostatistics, computational analysis): M. Zhang, N. Kobayashi, K.A. Zettlitz, R.E. Reiter.

Writing, review, and/or revision of the manuscript: M. Zhang, N. Kobayashi, K.A. Zettlitz, W.K. Tsai, J. Yamashiro, E.A. Kono, A.M. Wu, R.E. Reiter.

Administrative, technical, or material support (i.e., reporting or organizing data, constructing databases): W.K. Tsai, K.A. Zettlitz, J. Yamashiro, E.A. Kono, C.P. Tran, C. Wang, J. Guan

Study supervision: M. Zhang, N. Kobayashi, K.A. Zettlitz

Disclosure of Potential Conflicts of Interest: A. Wu and R. Reiter are co-founders of ImaginAb, Inc. and hold equity. A. Wu is a consultant/advisory board member for ImaginAb, Inc. No potential conflicts of interest were disclosed by the other authors.

Results: A11 Mb was successfully conjugated with IRDye800CW and retained specific binding to PSCA. *In vivo* imaging showed maximal signal to background ratios at 48 hours. The A11 Mb-IRDye800CW specifically detected PSCA positive primary tumors, tumor infiltrated lymph nodes, and distant metastases with high contrast. Fluorescence guidance facilitated more complete tumor resection, reduced tumor recurrence, and improved overall survival, compared with conventional white light surgery. The probe successfully identified primary orthotopic tumors and metastatic lesions in hPSCA transgenic mice.

Conclusions: Real-time fluorescence image-guided surgery with A11 Mb-IRDye800CW enabled detection of lymph node metastases and positive surgical margins, facilitated more complete tumor removal, and improved survival, compared to white light surgery. These results may be translatable into clinical practice to improve surgical and patient outcomes.

Introduction

Prostate cancer is among the most prevalent male malignancies worldwide. It represents the second leading cause of cancer-related death for men in the United States (1). Radical prostatectomy remains one of the mainstays of treatment for localized prostate cancer. Complete tumor resection is critical for optimal cancer management. Positive surgical margins increase the likelihood of tumor recurrence and the need for secondary treatments such as adjuvant or salvage radiation, which may impact overall survival in some patients (2–4). However, extracapsular extension of prostate cancer is rarely visible during prostatectomy even under extreme magnification, and extended resection risks injury to surrounding tissues that may lead to urinary incontinence and sexual impotence (5,6). Therefore, there is an urgent need for technologies that can aid visualization of tumor boundaries intraoperatively, which may reduce the incidence of positive surgical margins while reducing surgical toxicity.

Prostate cancer metastasizes most commonly to regional and distant lymph nodes (LN), and detection of positive LNs may impact subsequent management (7,8). Complete removal of involved regional nodes may also impact disease progression (9). However, there is currently no reliable way to detect and remove metastatic nodes intraoperatively. As many as 35% of involved nodes are located outside of traditional surgical templates (10), and the variability of nodal spread has made reliable identification of sentinel nodes difficult. Although improved molecular imaging with PET (e.g. PSMA, FACBC, and choline) may identify men with lymphatic involvement, PET may understage patients (11–13). Additionally, there is no simple way to identify the PET-visualized LNs intraoperatively. Therefore, an intraoperative navigation system or probe that can visualize cancer-bearing LNs and facilitate complete excision could impact prostate cancer management and clinical outcome.

An increasing number of investigators have endeavored to improve tumor detection and visualization with radioactive and optical probes (14,15). Hand-held gamma detectors that detect the drainage of intraprostatically injected Technetium-99m have been employed in prostate cancer surgical procedures with only modest efficacy given the variable drainage pattern of the prostate (16). Technetium-labeled small molecules targeting PSMA are also being explored (17). Fluorescent probes, such as intraprostatic indocyanine green (ICG),

have also been administered in the peritumoral location to identify sentinel nodes during surgery with only modest success (18).

In the present study, we employed a humanized engineered minibody that targets the cell surface protein PSCA (A11 Mb). Antibody fragments such as the minibody retain the binding specificity of the parental antibody but exhibit faster tumor uptake and more rapid clearance from non-target tissues to produce high contrast images (19). PSCA is over-expressed in 83–100% prostate cancer and higher levels correlate with poor prognosis, LN spread, and metastatic disease (20,21). Importantly, PSCA expression in normal tissues is highly restricted with no expression in bone marrow or LNs, common sites of prostate cancer metastasis (22). A11 Mb was labeled with the near-infrared (NIR) fluorescent dye IRDye800CW and evaluated for binding to PSCA-expressing prostate cancer cells *in vitro* and *in vivo*. In particular, we examined the ability of the A11 Mb-IRDye800CW to detect primary tumors and LN metastases in xenograft models and in a novel transgenic mouse model expressing the human PSCA gene. Finally, we evaluated the clinical potential of A11 Mb-IRDye800CW to provide surgical guidance and thereby to reduce the incidence of positive surgical margins, local recurrence, and to improve survival.

Material and methods

Reagents

A11 Mb, an engineered antibody fragment (scFv-C_H3 homodimer, 80 kDa), was developed and validated for preclinical *in vivo* targeting of PSCA at UCLA (23). Detailed biodistribution data for the A11 Mb was previously determined (24). IRDye800CW NHS ester (IRDye) (773 nm absorbance, 792 nm emission) was purchased from LI-COR Biotechnology (NE, USA, Cat# 929–70020).

Conjugation of A11 Mb-IRDye800CW probe

The IRDye800CW fluorophore was conjugated with A11 Mb using NHS ester chemistry. Indicated molar excess of fluorescent dyes were incubated with 1 mg/mL A11 Mb in 0.1 M Na_2HPO_4 buffer (pH=8.6) at room temperature for 2 hours. Excess free dye was removed using a Micro Bio-Spin™P6 column (Bio-Rad, #7326221) according to the manufacturer's instruction. The final concentrations of conjugated product were measured photometrically by NanoDrop2000C spectrophotometer. The number of fluorophore molecules conjugated to each minibody molecule was calculated from IRDye800CW (780 nm) and protein (280 nm) concentrations. Sodium dodecyl sulfate polyacrylamide gel electrophoresis (SDS-PAGE) was used to verify the conjugation. The probe was stored at 4°C.

Size exclusion chromatography

Size exclusion chromatography was performed using a Superdex200 10/300GL column (GE Healthcare Life Sciences) on an ÄKTA Purifier (GE Healthcare Life Sciences) with PBS as mobile phase at a flow rate of 0.5 mL/minute. Absorbances at 280 nm for protein and at 780 nm for IRDye800CW were monitored during elution. β-Amylase (200 kDa), carbonic anhydrase (29 kDa), and cytochrome C (12.4 kDa; Sigma-Aldrich, Saint Louis) were used as protein molecular weight standards.

Cell culture

CWR22Rv1 cells were obtained from American Type Culture Collection (ATCC, Manassas, VA) and cultured in RPMI 1640 medium containing 10% fetal bovine serum (FBS), 1 × sodium pyruvate and 1% Penicillin-Streptomycin-Glutamine (PSG). PC3 cells (ATCC) were cultured in the Dulbecco modified Eagle medium (DMEM) with 5% FBS + 1% PSG. The mouse prostate cancer cell line RM9 and RM9-PSCA-Firefly-Luciferase (Fluc) cells were provided by University of Texas MD Anderson Cancer Center and Dr. Saul Priceman (City of Hope). RM9 cells were grown in DMEM supplemented with 10% FBS + 1% PSG. 22Rv1-PSCA and PC3-PSCA were generated to express PSCA as previously described and cultured in the same media as mentioned for the parental cell lines above (23). Fluc-expression-lentivirus was purchased from UCLA Vector Core and used to transduce 22Rv1, 22Rv1-PSCA, PC3, PC3-PSCA, and RM9 cells. All cells were maintained in a humidified incubator at 37°C and 5% CO_2.

Flow cytometry analysis

22Rv1-PSCA and 22Rv1 cells were detached from plates with glucose-EDTA, stained with A11 Mb-IRDye800CW (1 μg per 1 × 10^6 cells) on ice for 2 hours, and washed with 2% FBS/PBS 3 times. A murine anti-human PSCA antibody, 1G8 (25), was used as a positive control with Alexa Fluor 647-goat-anti-mouse IgG secondary antibody (Invitrogen). A11 Mb-IRDye800CW binding to PSCA-expressing cells was tested using PC3-PSCA, PC3 cells, RM9-PSCA and RM9 cells by flow cytometry as described above.

To determine the apparent affinity of A11 Mb-IRDye800CW, 5 × 10^5 22Rv1-PSCA and 22Rv1 cells were incubated with A11 Mb-IRDye800CW (dye-to-protein ratio 0.5) at concentrations ranging from 0 to 512 nM in 200 μL of 2% FBS/PBS, for 3 hours at 4°C in triplicate. The mean fluorescence intensity of each sample was fitted to a one-site saturation-binding model. Acquisition was performed with an LSRFortessa X-20 SORP flow cytometer (BD Biosciences) and analysis was performed with FlowJo 9.3.2. (TreeStar).

Human PSCA knock in mouse

The human PSCA knock in (hPSCA-KI) mouse model was generated by targeted insertion of hPSCA cDNA into the murine PSCA gene through homologous recombination in the murine embryonic stem cells by standard gene-targeting methods (Supplementary Fig. S4). The hPSCA-KI mouse model is established by backcrossing with C57BL/6J for 6 generations. PCR primers (5′ to 3′) for genotyping were as follows; sense strand, mP-F6, TGTCACTGTTGACTGTGGGTAGCA; antisense strand, mP3-R1, CTTACTTGATAGGAGGGCTCAGCA, and hPSCA-1 3', CCAGAGCAGCAGGCCGAGTGCA). PCR was performed with Taq DNA polymerase (Invitrogen) with 35 cycles of denaturation at 94 °C for 25 s, annealing at 59.5 °C for 25 s, and elongation at 72 °C for 45 s.

Quantitative RT-PCR

Total RNA was isolated from various organs of hPSCA-KI mice using RNeasy mini kit (Qiagen). One μg of total RNA was reverse transcribed and semi-quantitative RT-PCR was

performed for human PSCA (30 cycles) and GAPDH (27 cycles; loading control) using Gene Amp RNA PCR kit (Applied Biosystem) according to the manufacture's protocol.

Bioluminescence imaging

Bioluminescence imaging (BLI) was performed using the IVIS Lumina II *In Vivo* Imaging system (PerkinElmer, MA, USA) to monitor tumor growth, tumor recurrence, and LN metastases. Mice were administered with 150 mg/kg D-luciferin in 100 μL of normal saline by intraperitoneal injection, and anesthetized with 2% isoflurane. BLI images were acquired 10 min after the D-luciferin injection. Living Image software (Xenogen) was used to quantify bioluminescence signals. The value of bioluminescence signals was quantified in units of radiance, photons per second per centimeter squared per steradian ($p/sec/cm^2/sr$).

Fluorescence imaging

A Maestro II small animal optical imaging system (Cambridge Research & Instrumentation, Woburn, MA) was used for fluorescence imaging. The NIR filter set was selected with the extinction band pass filter at 684 to 729 nm, the emission filter at 745 nm longpass, and the acquisition settings from 740 to 950 nm in 10 nm steps. A11 Mb-IRDye800CW probe was injected through the lateral tail vein at 25 μg per mouse. Imaging was performed at 48 hours post injection (p.i.), or otherwise as indicated. Mice were anesthetized with 2% isoflurane at each imaging session for serial imaging at multiple time points. The fluorescent signals were unmixed and then measured using the software version 2.10 provided by the manufacturer (CRI, Maestro). The fluorescence intensity of PSCA+ tumor was compared to the PSCA- tumor in the same tumor-bearing mouse.

Xenograft and transgenic knock-in mouse models

All animal experiments, housing, breeding, surgical procedures including pre- and post-operative care and analgesics administration were conducted in compliance with protocols approved by the Chancellor's Animal Research Committee at UCLA. Five to 8-week-old male athymic nude mice (Charles River Laboratories), SCID mice (Taconic Biosciences) and C57BL/6 mice (Jackson Laboratory) were purchased. Mice were fed irradiated alfalfa-free rodent diet (Envigo Teklad, Madison, WI) to reduce nonspecific fluorescent signals in stomach and gut for one week prior the imaging experiments.

Subcutaneous model: 1×10^6 22Rv1-Fluc and 22Rv1-PSCA-Fluc cells in 100 μL Matrigel/PBS (1:1, v/v, Corning) were injected subcutaneously in the flank of nude mice. For each mouse, the parental tumor was implanted on the left flank and PSCA+ tumor on the right. Tumor growth was monitored by caliper measurements. When tumors reached about 15 mm in diameter (10–14 days after injection), fluorescence imaging experiments were conducted.

LN metastasis model: 5×10^5 PC3-PSCA-Fluc cells in 40 μL PBS were injected into the left hock of SCID mice. BLI was performed weekly to monitor the tumor growth and metastases. When LN metastases were detected by BLI (about 7 weeks after the inoculation), fluorescence imaging experiments were conducted.

Intracardiac model: 1×10^5 PC3-PSCA-Fluc cells in 100 μL saline solution was injected into the left ventricle of SCID mice. Tumor establishment and metastases were monitored by BLI once a week. When multiple metastatic lesions were detected by BLI, A11 Mb-IRDye800CW probe was injected and fluorescence imaging was conducted at 48 hours post injection.

Intramuscular model: 1×10^6 22Rv1-PSCA-Fluc cells in 50 μL media/Matrigel (1:1, v/v, Corning) were injected into the posterior thigh muscle of the right leg in 20 nude mice, as previously described (26). BLI was used to monitor the tumor growth.

Transgenic knock-in mouse model: 1×10^6 RM9 and RM9-PSCA-Fluc cells in 100 μL Matrigel/PBS (1:1, v/v, Corning) were injected into the bilateral flank of hPSCA–KI mice to establish the subcutaneous tumor model as described above. For the orthotopic tumor model, 5×10^4 RM9-PSCA-Fluc cells in 5 μL PBS/Matrigel (1:1, v/v, Corning) were injected into dorsal prostate lobes of hPSCA-KI mice. Tumor growths were monitored by BLI.

Fluorescence-guided survival surgery of intramuscular 22Rv1-PSCA-Fluc tumors

For the resection surgery of intramuscular 22Rv1-PSCA-Fluc tumors, twenty tumor-bearing nude mice were injected with 25 μg A11 Mb-IRDye800CW probe 48 hours prior to the operation. Mice were anesthetized with a ketamine/xylazine mixture via intraperitoneal injection. The mice were randomized into two cohorts (n=10 in each cohort), which received either tumor resection surgery under white light or white light surgery followed by fluorescence-guided surgery. The surgeon was blinded to the groupings while performing the first-round white light surgery. In one cohort, the secondary fluorescence-guided surgery was conducted to resect the residual tumors using a fluorescence dissecting microscope (Leica M205 FA, Leica Microsystems) at 10× magnification. Images of the fluorescent signal and surgical video were captured by a Leica DFC 9000GT monochrome camera with a filter for IRDye800 (excitation 710/75 nm and emission 810/90 nm) and displayed on an adjacent computer monitor during surgery. Images were analyzed with the use of Leica Application Suite X software. After surgery, any residual fluorescent tissue and/or tumor margins were surgically collected for histologic analysis. Non-fluorescent tissue margin was also collected as control. Mice were monitored and followed by BLI every 10 days post operation. When the recurrent tumor reached 15 mm in diameter or mice's mobility was impaired, the mice were euthanized in accordance with our Animal Research Committee protocol to reduce unnecessary stress.

Immunohistochemisty

Tissue samples were fixed in formalin, paraffin-embedded (FFPE), sectioned, and stained with Hematoxylin and Eosin (H&E) by the UCLA pathology core facility. Four-μm thick sections from the FFPE samples were used for Immunohistochemical (IHC) analyses using M.O.M. immunodetection kit (Vector, BMK-2202) according to the manufacture's manual with modifications as follows. The tissue slides were incubated with the mouse IgG blocking reagent for 1 hour at room temperature, followed by incubation overnight with the anti-human PSCA primary antibody (Abcam, ab56338) at 4°C, and biotinylated anti-mouse

secondary antibody (Vector, BMK-2202) at room temperature for 20 min. The slides were washed with PBS + 0.1% Tween 20 (PBST) for 5 min three times after each antibody incubation. The slides were counter stained with Hematoxylin. The image was captured by Olympus microscope (BX41).

Statistic analysis

All quantitative data were represented as mean ± SD. The two-tailed student's *t* test was used for normally distributed values between two group comparisons, while Mann-Whitney U test was performed for variables without normal distribution. Kaplan-Meier analysis was used to determine the mice survival and differences between two treatment groups. Statistical analyses were performed with GraphPad Prism (version 6.0, GraphPad Software, Inc.). $P < 0.05$ was considered statistically significant.

Results

Development and characterization of A11 Mb-IRDye800CW

IRDye800CW NHS ester was conjugated to surface exposed lysine residues on the engineered anti-PSCA A11 Mb (Fig. 1A). Because dye conjugation can impact the biodistribution and plasma clearance of the protein, we tested two different dye-to-protein (D:P) molar ratios. Two and five-fold molar excess of IRDye800CW relative to A11 Mb produced final D:P ratios 0.5 and 1.1, respectively. Successful conjugation was shown by the specific 80 kDa fluorescent bands (red) corresponding to the Coomassie blue stained bands of the same apparent molecular weight on a SDS-PAGE gel (Fig. 1B). The 5:1 conjugation reaction yielded a brighter band compared to the 2:1 reaction. The unconjugated A11 Mb was not visible by fluorescence imaging, as expected.

Purity and integrity of the A11 Mb-IRDye800CW were evaluated by size exclusion chromatography. The unconjugated A11 Mb and A11 Mb-IRDye800CW (both D:P ratios at 0.5 and 1.1) eluted as a single elution peak with similar retention times (27.2 and 27.1 minutes, respectively), indicating that IRDye800CW conjugation did not interfere with dimeric minibody conformation and that the probe was not aggregated (Fig. 1C). The specificity of the minibody and its parental antibody has been reported extensively in prior work (23–25,27,28). Flow cytometry showed specific binding of the A11 Mb-IRDye800CW probe to 22Rv1-PSCA, with an apparent affinity of 26.5 ± 3.0 nM. The selectivity of A11 Mb-IRDye800CW for PSCA was demonstrated by lack of binding to PSCA-negative parental 22Rv1 cells (Fig. 1D and E). Similarly, PSCA-specific binding of the probe to PC3-PSCA and RM9-PSCA cells was confirmed by flow cytometry, whereas there was no binding to the PSCA-negative parental PC3 and RM9 lines (Supplementary Fig. S1).

Determination of optimal imaging parameters

We evaluated the *in vivo* specificity of the A11 Mb-IRDye800CW probe in PSCA-positive 22Rv1-PSCA-Fluc and PSCA-negative 22Rv1-Fluc xenografts. Mice implanted with 22Rv1-PSCA-Fluc and 22Rv1-Fluc cells formed bioluminescent tumors after two weeks (Fig. 2A and B). A dose ranging experiment for the A11 Mb-IRDye800CW in *in vivo* imaging showed that increasing the amount of A11 Mb-IRDye800CW resulted in increasing

fluorescent signals specific to PSCA+ tumors (Supplementary Fig. S2). The dosage of A11 minibody at 25 ug protein (1 mg/kg) had been shown as a safe and effective dose in our previous reports (24,28), and was used for the present study. Fluorescence imaging (extinction, 684 to 729 nm; emission, 789nm; acquisition, 740 to 950 nm) after i.v. injection of 25 μg A11 Mb-IRDye800CW visualized PSCA-expressing tumors clearly, whereas PSCA-negative tumors were not visible (Fig. 2C). D:P ratios may affect the affinity, biodistribution, and non-specific retention of A11 Mb-IRDye800CW. We compared A11 Mb-IRDye800CW with the final D:P ratio 0.5 and with the final D:P ratio 1.1 by imaging the mice with 22Rv1-PSCA-Fluc and PSCA-negative 22Rv1-Fluc xenografts (n=5 in each group). At 48 hours after probe injection, higher contrast was seen for the probe with a D:P ratio of 0.5 (PSCA positive to negative signal ratio of 4.01 ± 1.14) compared to the probe with a D:P ratio of 1.1 (PSCA positive to negative signal ratio of 1.94 ± 0.43) (Fig. 2D), suggesting that a lower D:P ratio of 0.5 led to the fluorescent images with higher contrast, while minimizing potential changes in pharmacokinetics of A11 Mb.

Serial imaging of tumor-bearing mice (24, 48, 72, 96 and 120 hours p.i.) determined the optimal time interval from probe injection to fluorescent imaging *in vivo*. Maximum florescence intensity and ratios of PSCA+ and PSCA– tumors were determined at all time points. Strong fluorescent signal was observed in PSCA+ tumors from 24 to 72 hours after injection, following which signal contrast diminished (Fig. 2E), suggesting that the probe could produce long-lasting signal and provide a sufficient time window for intraoperative imaging. The maximal PSCA+ to PSCA-negative tumor fluorescence ratio was reached at 48 hours p.i. (Fig. 2F and G), which formed the basis for all future experiments.

Detection of lymphatic and distant metastases *in vivo* using A11 Mb-IRDye800CW

We next tested the ability of the A11 Mb-IRDye800CW probe to detect lymphatic and distant metastatic lesions, reasoning that *in vivo* visualization of regional and metastatic spread could guide surgical resection and potentially improve surgical outcomes in high-risk disease. To demonstrate the ability of A11 Mb-IRDye800CW to detect LN metastases, we established a novel LN metastasis model by hock injection of PC3-PSCA-Fluc cells in SCID mice. BLI detected metastases seven weeks after tumor inoculation (Fig. 3A). As shown in Figure 3B, multiple tumor-infiltrated LNs (popliteal LN, sciatic LN, lumbar LN, and medial iliac LN) were clearly visualized by PSCA-targeted A11 Mb-IRDye800CW fluorescence imaging. While most fluorescent-positive nodes appeared enlarged and could be found under white light at autopsy, we also detected subclinical metastases in normal appearing LNs less than one millimeter in diameter, such as the external iliac LN shown in Figure 3B and 3C. Tumor cell invasion in the fluorescence-positive LNs was further confirmed by *ex vivo* BLI of the resected LN (Fig. 3C), as well as by histological examination (Fig. 3D and E). These results demonstrate that A11 Mb-IRDye800CW can sensitively detect LN metastases.

Furthermore, A11 Mb-IRDye800CW was used to detect additional sites of metastasis established by intracardiac injection of PC3-PSCA-Fluc cells. At six weeks post injection, distant metastases were detected by BLI. Fluorescence imaging was performed 48 hours after administration of A11 Mb-IRDye800CW. For postmortem imaging, the skin was removed to reduce auto-fluorescence and to mimic an intraoperative setting. Multiple distant

metastases were visualized as shown in Fig. 4A. Fluorescent signal in the liver represents minibody clearance and autofluorescence. Notably, PSCA-guided fluorescence imaging identified multiple metastases *in vivo*, including the tumor embedded in the left thigh muscle under the fat tissue, which would have been overlooked on bright field imaging (Fig. 4A). All metastatic tumor lesions were resected and confirmed by fluorescence *ex vivo* (Fig. 4B), as well as by histological examination (Fig. 4C). These results suggest that the NIR signal generated by A11 Mb-IRDye800CW could enhance the ability of surgeons to find metastases intraoperatively, much as it enabled visualization of regional LNs.

Surgical resection with real-time fluorescence guidance improves recurrence-free survival

To assess the potential utility of PSCA-targeted imaging with A11 Mb-IRDye800CW to aid tumor resection and improve recurrence-free survival, we compared surgical resection of prostate cancers by white light surgery alone to combined white light and fluorescence-guided surgery in a prospective, randomized study. We engrafted 22Rv1-PSCA-Fluc cells intramuscularly into nude mice (n=20), which produced deeply invasive, difficult to resect tumors. Two weeks after tumor inoculation, tumor-bearing mice (confirmed by bioluminescence) were randomized into two groups with equal average preoperative tumor burdens (Fig. 5A and B). Forty-eight hours p.i., a surgeon blinded to treatment group resected all tumors under white light, attempting to resect tumor completely while preserving normal tissues (akin to radical prostatectomy). Following white light resection, mice randomized to the fluorescence cohort underwent a second surgery to remove fluorescing tissue. As shown in Fig. 5C, tumors were deeply invasive and the borders between tumor and surrounding tissues were not easily distinguishable under white light. In comparison, intraoperative fluorescence imaging facilitated clear visualization of residual fluorescing tumors. We could distinguish nearby neurovascular structures from tumor and achieve complete tumor resection (Supplementary Fig. S3 and Video S1). Bioluminescent imaging 10 days after resection demonstrated that fluorescence-guided surgery resulted in more complete tumor removal compared to white light surgery alone. At this point, 8 of 10 mice in the white light surgery group showed detectable bioluminescence, whereas none of the mice in the fluorescence-guided surgery group showed residual signal (Fig. 5A). Bioluminescence of tumor burden as measured using region of interest (ROI) analysis was significantly lower in the group that had undergone the fluorescence guided surgery ($p<0.001$). These differences in tumor burden were more significant at 20 days post-operation (Fig. 5B). Histopathological examination of the surgical margins of the thigh musculature (taken at the time of surgery) confirmed the presence of residual tumor in the white light group but not the fluorescence group (Fig. 5D). Significantly, the lower positive margin and decreased recurrence rate translated into an overall survival advantage among mice that received combined white light and fluorescence surgery. The median survival for the white light surgery group was 24 days, whereas 90% of mice in the fluorescence-guided resection group survived with no evidence of tumor recurrence at the conclusion of the study at day 70 ($p<0.001$) (Fig. 5E).

A11 Mb-IRDye800CW fluorescence-guided surgical resection was also performed in SCID mice that developed PC3-PSCA-fluc metastatic LNs via hock injection. Real-time intraoperative fluorescence imaging provided identification of LNs with metastasis and

facilitated surgical resection without injury to adjacent nerves (Supplementary Fig. S4 and Video S2).

Imaging orthotopic and metastatic tumors with A11 Mb-IRDye800CW in a human PSCA knock-in mouse

One limitation of PSCA-specific antibody imaging in immunodeficient mouse models is that A11 minibody does not cross-react with the murine PSCA homologue, and whether binding of A11 Mb-IRDye800CW to normal tissue expressing PSCA could interfere with image contrast and hence impair surgical resection cannot be assessed. To evaluate A11 Mb-IRDye800CW fluorescence imaging in the context of normal PSCA expression, we employed a genetically engineered mouse model in which the human PSCA gene had been introduced into the murine PSCA locus. As predicted based on the distribution of PSCA in normal human and murine tissues, endogenous hPSCA mRNA was detected in stomach, bladder and prostate (Supplementary Fig. S5). RM9, a syngeneic mouse prostate cancer cell line, was engineered to express hPSCA and Fluc and implanted subcutaneously (n=5, Supplementary Fig. S6) and orthotopically (n=8) into hPSCA-KI mice (both homozygous and heterozygous males were used). Once tumor growth was detected by bioluminescence, the mice were administered A11 Mb-IRDye800CW and euthanized 48 hours later. Fluorescence-imaging of hPSCA-KI mice bearing bilateral subcutaneous tumors showed strong signal in RM9-PSCA-Fluc tumors while no signal was detected in the control PSCA-negative RM9 tumors (Supplementary Fig. S6). The mice with orthotopic tumors were opened to expose the pelvic organs in order to simulate surgery. *In situ* NIR fluorescence imaging detected fluorescent signals in the antigen-positive tumors with high tumor to background contrast (Fig. 6A and Supplementary Fig. S6). Furthermore, in the orthotopic tumor model, fluorescence imaging clearly revealed the presence of LN metastases (mesentery and lumbar LNs), supporting the hypothesis that intraoperative imaging can be used to identify regional and distant LN metastases. Next, we evaluated the probe's biodistribution by harvesting the major organs, prostate, and metastatic lesions and examining them with *ex vivo* fluorescence imaging. As shown in Fig. 6B, the prostate (with cancer), metastatic LNs, liver, kidneys, and stomach emitted fluorescent signals, while the other organs and tissues (lung, heart, spleen, bone, pancreas, muscle) showed no significant fluorescence. Fluorescent signals in liver, kidney, and bladder are due to metabolism and urinary excretion of the probe, although some bladder fluorescence is attributable to endogenous expression (Supplementary Figure. S7). The strong signal in stomach was due in part to auto-fluorescence of food contents in the stomach despite use of alfalfa-free pellets, although again some signal is attributable to expression of PSCA in stomach mucosa (Supplementary Fig. S7). Finally, histology and immunohistochemical staining for PSCA confirmed the presence of cancer in the prostate and involved LNs (Fig. 6C). These results demonstrate the ability of A11 Mb-IRDye800CW to detect local and metastatic prostate cancers *in vivo* in a model most analogous to patients with prostate cancer.

Discussion

Effective intraoperative image-guided surgery is a major unmet need in the management of men with prostate cancer. Fluorescence-image guided surgery is one of the most promising

methodologies to improve disease visualization, aiding tumor identification and complete resection, while avoiding injury to adjacent normal tissues such as the neurovascular bundles in the case of prostate cancer. Recent reports have demonstrated successful utilization of intraoperative fluorescent probes for imaging of tumors and in sentinel lymph node mapping of various types of cancer (29–31).

Here, we conjugated the NIR dye IRDye800CW to the anti-PSCA antibody fragment, A11 Mb, and tested whether fluorescence-imaging with A11 Mb-IRDye800CW could aid in resection of a locally invasive prostate tumor during surgery, decrease tumor recurrence, and improve prognosis. While it is not technically feasible to perform radical prostatectomy in mouse models, the deeply invasive intramuscular tumor model we used does recapitulate important features of radical prostatectomy, such as the difficulty of margin visualization under white light. Special attention was paid to conduct unbiased surgery blinded to the groupings during the first round of standard surgery under white light with the goal of removing as much tumor as possible while preserving adjacent normal tissues, akin to radical prostatectomy. The post-operative bioluminescence imaging studies clearly showed that more complete resection of cancer tissue was achieved by fluorescent image-guided surgery (FIGS). Our results demonstrate that the new NIR probe clearly delineated between antigen-expressing tumor and healthy surrounding tissues, allowing the surgeon to precisely visualize tumor margins and achieve more complete tumor resection. This in turn led to a lower residual tumor burden, reduced recurrence, and ultimately significantly improved overall survival.

We previously reported that intraoperative fluorescent guidance with a Cy5 labeled PSCA diabody fragment (scFv dimer) could also enable detection of residual tumor and reduce positive surgical margins (26). In this study, IRDye800CW was selected because of its preliminary success in clinical studies due to its low auto-fluorescence and high spatial resolution (32,33). Rosenthal and colleagues evaluated anti-EGFR cetuximab-IRDye800CW in patients with head and neck cancer. Cetuximab-IRDye800CW was well-tolerated and provided robust fluorescence contrast between tumor and normal tissue during intraoperative surgical resection (32). More recently, Lamberts and colleagues injected bevacizumab-IRDye800CW intravenously into patients with primary breast cancer, targeting VEGF-A. The group demonstrated the safety and feasibility of a NIR fluorescent probe to improve tumor margin detection intraoperatively (33). In addition to its safety, NIR fluorescent emission can be captured with frame rates of up to 30fps, which is ideal for real-time detection. Perhaps most importantly, IRDye800CW is compatible with existing laparoscopic and robotic surgical systems, which may facilitate clinical translation of this probe.

We selected the 80 kDa minibody format for this study for a number of reasons. First, anti-PSCA A11 minibody was capable of binding specifically PSAC-expressing tumors after conjugation with IRDye800CW, as shown by flow-cytometry study and by PSCA-specific fluorescent signals detected *in situ* and *ex vivo* compared to PSCA-negative control tumors and organs. A11 Mb-IRDye800CW *in vivo* imaging was able to produce PSCA-specific fluorescent signals with high contrast for all three cell lines used in the study that express PSCA at various levels; the PC3-PSCA and 22Rv1-PSCA cell lines have PSCA cell-surface density 5.2×10^5 antigens/cell and 2.1×10^6 antigens/cell, respectively; RM9-PSCA cells has

lower PSCA expression than 22Rv1-PSCA as determined by IHC and flow cytometry (data not shown). Importantly, the range of PSCA expression levels are comparable to the expression observed in prostate cancer patient samples. Second, the fast tumor uptake and the more rapid clearance from non-target tissues of A11 minibody compared to the parental antibody can provide practical time window for surgery. A 1–3 day window offers flexibility in scheduling and performance of probe injection and surgical procedure. Additionally, the engineered antibody fragment can be labeled with more than a single moiety. Tsai et al. have adapted the A11 minibody for dual PET and fluorescent imaging, which could allow for upfront PET imaging to localize tumor, followed by fluorescence guidance to identify and resect those lesions (34) (Tsai *et. al*, manuscript in preparation).

Lymphatic drainage is a major route of tumor dissemination in prostate cancer. The ability to detect nodal metastases and achieve complete nodal resection in patients with high-risk disease in the operating room are major unmet clinical needs for prostate cancer. Various fluorescent imaging probes have been developed to better visualize and characterize the lymphatic system. The NIR dye, ICG, has been extensively studied for intraoperative sentinel LN mapping in a variety of tumors such as skin, breast, and gastrointestinal cancers (35–37). In patients with cervical cancer, ICG showed sentinel node identification rates comparable with conventional radiotracers and blue dyes (38). However, the non-tumor-specific properties make this dye less than ideal for real-time visualization of metastatic tumor lesions. Recently, Cai and colleagues developed Alexa Fluor 680-conjugated bombesin (BBN) peptides against the gastrin releasing peptide receptor (GRPR), and detected LN metastases in mouse models. Fluorescence imaging with BBN-Alexa Fluor 680 was performed for up to 6 hours after post injection (39). In the current study, we established a prostate xenograft mouse model with multiple lymph node metastases via hock injection. The tumor infiltrated LNs, including small nodes with early stage microscopic metastasis that may be easily overlooked by gross examination, were clearly detected by A11 Mb-IRDye800CW after systemic administration into the mice. The smallest size of affected lymph node (external iliac LN) imaged by A11 Mb-IRDye800CW was only 1mm in diameter and it was not distinguishable from normal nodes. The result indicates the potential of FIGS with A11 Mb-IRDye800CW in resecting tumors that are too small to identify as nodal disease at all, or as pathological nodal disease. One of the challenges of developing effective lymphatic imaging agents is delivering the probe into the lymph nodes. A11 Mb-IRDye800CW showed stable retention in lymph nodes due to the specific binding to tumor cells mediated by the antibody fragment. These advantages were confirmed in our study, demonstrating the suitability of the probe for detection and resection of involved lymph nodes. The potential use of the probe in assisting in identifying residual disease for salvage pelvic node dissections is noteworthy.

PSMA ligand PET imaging is becoming recognized as a powerful tool for detection of a recurrent PCa and for nodal and bone metastases for high-risk primary PCa (40). While PSMA-targeted fluorescent imaging is possible, the current generation of PET probes are small molecules whose binding may be hindered by a large optical moiety such as IRDye800. PSCA-directed intraoperative imaging could be used in conjunction with either a PSCA PET probe or any of the current PSMA PET probes. In addition to a majority of

prostate cancers, PSCA is also expressed by other malignancies such as pancreatic, bladder, and ovarian cancers, to which A11 Mb-IRDye800CW FIGS may be applied.

A unique feature of this study was our evaluation of A11 Mb-IRDye800CW in a transgenic mouse that expresses hPSCA. This distribution of PSCA in this mouse model was concordant with that in humans (stomach, bladder, prostate). Primary tumor and metastatic lesions were clearly distinguishable from background with a high signal-to-background ratio. Although hPSCA KI mice had low-level expression of PSCA in the normal mucosa of the stomach as determined by IHC and mRNA expression (41), imaging of the surgical area with A11 Mb-IRDye800CW was not interfered by the fluorescence in the stomach because of the distance between the two organs. In contrast, the bladder had strong fluorescent signal, although this was largely caused by clearance of the probe through the kidney. Residual signal from the bladder after removal of urine was faint, consistent with weak and spotty expression seen by immunohistochemistry. Diuresis or catheterization could be used to clear bladder signal during surgery in order to avoid any potential loss of contrast at the level of the bladder neck. These results demonstrate the feasibility of the A11 Mb-IRDye800CW for fluorescence imaging, intraoperatively distinguishing local, loco-regional and metastatic prostate cancer from normal tissue. In the present study, we explored the sensitivity, specificity, and utility of fluorescent imaging in multiple models, including distant lymph nodes and other soft tissue metastases. We can envision changes in practice with the advent of better PET imaging that may lend themselves to fluorescent imaging and complete surgical resection of distant metastases. The development of novel targeted fluorescent probe has the potential to transform the surgical landscape of prostate cancer, particularly in the age of robotics and cameras capable of detecting fluorescent images.

Supplementary Material

Refer to Web version on PubMed Central for supplementary material.

Acknowledgements:

In vivo fluorescence imaging was performed at the California Nano-Systems Institute Advanced Light Microscopy/Spectroscopy and the Macro-Scale Imaging Shared Facilities at UCLA.

Grant Support: This work was supported by NIH grants R01 CA174294, P30 CA016042, UCLA SPORE in Prostate Cancer 5P50CA092131–12, and Department of Defense W81 XWH-15–1-0725. Imaging, flow cytometry, pathology core services were supported by Jonsson Comprehensive Cancer Center (P30 CA016042).

References

1. Siegel RL, Miller KD, Jemal A. Cancer statistics, 2016. CA: a cancer journal for clinicians 2016;66(1):7–30. [PubMed: 26742998]
2. Chalfin HJ, Dinizo M, Trock BJ, Feng Z, Partin AW, Walsh PC, et al. Impact of surgical margin status on prostate-cancer-specific mortality. BJU international 2012;110(11):1684–9. [PubMed: 22788795]
3. Stephenson AJ, Eggener SE, Hernandez AV, Klein EA, Kattan MW, Wood DP Jr., et al. Do margins matter? The influence of positive surgical margins on prostate cancer-specific mortality. European urology 2014;65(4):675–80. [PubMed: 24035631]

4. Izard JP, True LD, May P, Ellis WJ, Lange PH, Dalkin B, et al. Prostate cancer that is within 0.1 mm of the surgical margin of a radical prostatectomy predicts greater likelihood of recurrence. The American journal of surgical pathology 2014;38(3):333–8. [PubMed: 24525503]
5. Hruby S, Englberger C, Lusuardi L, Schatz T, Kunit T, Abdel-Aal AM, et al. Fluorescence Guided Targeted Pelvic Lymph Node Dissection for Intermediate and High Risk Prostate Cancer. The Journal of urology 2015;194(2):357–63. [PubMed: 25896557]
6. Saika T, Miura N, Fukumoto T, Yanagihara Y, Miyauchi Y, Kikugawa T. Role of robot-assisted radical prostatectomy in locally advanced prostate cancer. International journal of urology : official journal of the Japanese Urological Association 2018;25(1):30–5. [PubMed: 28901630]
7. Vilaseca A, Nguyen DP, Touijer KA. Should Fluorescence Mapping be Used to Guide Pelvic Lymph Node Dissection? The Journal of urology 2015;194(2):280–1. [PubMed: 25986512]
8. Chennamsetty A, Zhumkhawala A, Tobis SB, Ruel N, Lau CS, Yamzon J, et al. Lymph Node Fluorescence During Robot-Assisted Radical Prostatectomy With Indocyanine Green: Prospective Dosing Analysis. Clinical genitourinary cancer 2017;15(4):e529–e34. [PubMed: 27939590]
9. Yuh B, Artibani W, Heidenreich A, Kimm S, Menon M, Novara G, et al. The role of robot-assisted radical prostatectomy and pelvic lymph node dissection in the management of high-risk prostate cancer: a systematic review. European urology 2014;65(5):918–27. [PubMed: 23721959]
10. Mattei A, Fuechsel FG, Bhatta Dhar N, Warncke SH, Thalmann GN, Krause T, et al. The template of the primary lymphatic landing sites of the prostate should be revisited: results of a multimodality mapping study. European urology 2008;53(1):118–25. [PubMed: 17709171]
11. Freitag MT, Radtke JP, Hadaschik BA, Kopp-Schneider A, Eder M, Kopka K, et al. Comparison of hybrid (68)Ga-PSMA PET/MRI and (68)Ga-PSMA PET/CT in the evaluation of lymph node and bone metastases of prostate cancer. European journal of nuclear medicine and molecular imaging 2016;43(1):70–83. [PubMed: 26508290]
12. Kanagawa M, Doi Y, Oka S, Kobayashi R, Nakata N, Toyama M, et al. Comparison of trans-1-amino-3-[18F]fluorocyclobutanecarboxylic acid (anti-[18F]FACBC) accumulation in lymph node prostate cancer metastasis and lymphadenitis in rats. Nuclear medicine and biology 2014;41(7): 545–51. [PubMed: 24816330]
13. Schwenck J, Rempp H, Reischl G, Kruck S, Stenzl A, Nikolaou K, et al. Comparison of (68)Ga-labelled PSMA-11 and (11)C-choline in the detection of prostate cancer metastases by PET/CT. European journal of nuclear medicine and molecular imaging 2017;44(1):92–101. [PubMed: 27557844]
14. Lutje S, Rijpkema M, Goldenberg DM, van Rij CM, Sharkey RM, McBride WJ, et al. Pretargeted dual-modality immuno-SPECT and near-infrared fluorescence imaging for image-guided surgery of prostate cancer. Cancer research 2014;74(21):6216–23. [PubMed: 25252911]
15. Bu L, Shen B, Cheng Z. Fluorescent imaging of cancerous tissues for targeted surgery. Advanced drug delivery reviews 2014;76:21–38. [PubMed: 25064553]
16. Stroup SP, Kane CJ, Farchshchi-Heydari S, James CM, Davis CH, Wallace AM, et al. Preoperative sentinel lymph node mapping of the prostate using PET/CT fusion imaging and Ga-68-labeled tilmanocept in an animal model. Clinical & experimental metastasis 2012;29(7):673–80. [PubMed: 22714690]
17. Hillier SM, Maresca KP, Lu G, Merkin RD, Marquis JC, Zimmerman CN, et al. 99mTc-labeled small-molecule inhibitors of prostate-specific membrane antigen for molecular imaging of prostate cancer. Journal of nuclear medicine : official publication, Society of Nuclear Medicine 2013;54(8): 1369–76.
18. Polom K, Murawa D, Rho YS, Nowaczyk P, Hunerbein M, Murawa P. Current trends and emerging future of indocyanine green usage in surgery and oncology: a literature review. Cancer 2011;117(21):4812–22. [PubMed: 21484779]
19. Holliger P, Hudson PJ. Engineered antibody fragments and the rise of single domains. Nature biotechnology 2005;23(9):1126–36.
20. Lam JS, Yamashiro J, Shintaku IP, Vessella RL, Jenkins RB, Horvath S, et al. Prostate stem cell antigen is overexpressed in prostate cancer metastases. Clinical cancer research : an official journal of the American Association for Cancer Research 2005;11(7):2591–6. [PubMed: 15814638]

21. Gu Z, Thomas G, Yamashiro J, Shintaku IP, Dorey F, Raitano A, et al. Prostate stem cell antigen (PSCA) expression increases with high gleason score, advanced stage and bone metastasis in prostate cancer. Oncogene 2000;19(10):1288–96. [PubMed: 10713670]
22. Raff AB, Gray A, Kast WM. Prostate stem cell antigen: a prospective therapeutic and diagnostic target. Cancer letters 2009;277(2):126–32. [PubMed: 18838214]
23. Knowles SM, Tavare R, Zettlitz KA, Rochefort MM, Salazar FB, Jiang ZK, et al. Applications of immunoPET: using 124I-anti-PSCA A11 minibody for imaging disease progression and response to therapy in mouse xenograft models of prostate cancer. Clin Cancer Res 2014;20(24):6367–78. [PubMed: 25326233]
24. Knowles SM, Zettlitz KA, Tavare R, Rochefort MM, Salazar FB, Stout DB, et al. Quantitative immunoPET of prostate cancer xenografts with 89Zr- and 124I-labeled anti-PSCA A11 minibody. Journal of nuclear medicine : official publication, Society of Nuclear Medicine 2014;55(3):452–9.
25. Gu Z, Yamashiro J, Kono E, Reiter RE. Anti-prostate stem cell antigen monoclonal antibody 1G8 induces cell death in vitro and inhibits tumor growth in vivo via a Fc-independent mechanism. Cancer Res 2005;65(20):9495–500. [PubMed: 16230414]
26. Sonn GA, Behesnilian AS, Jiang ZK, Zettlitz KA, Lepin EJ, Bentolila LA, et al. Fluorescent Image-Guided Surgery with an Anti-Prostate Stem Cell Antigen (PSCA) Diabody Enables Targeted Resection of Mouse Prostate Cancer Xenografts in Real Time. Clin Cancer Res 2016;22(6):1403–12. [PubMed: 26490315]
27. Leyton JV, Olafsen T, Lepin EJ, Hahm S, Bauer KB, Reiter RE, et al. Humanized radioiodinated minibody for imaging of prostate stem cell antigen-expressing tumors. Clin Cancer Res 2008;14(22):7488–96. [PubMed: 19010866]
28. Lepin EJ, Leyton JV, Zhou Y, Olafsen T, Salazar FB, McCabe KE, et al. An affinity matured minibody for PET imaging of prostate stem cell antigen (PSCA)-expressing tumors. Eur J Nucl Med Mol Imaging 2010;37(8):1529–38. [PubMed: 20354850]
29. Chen Y, Dhara S, Banerjee SR, Byun Y, Pullambhatla M, Mease RC, et al. A low molecular weight PSMA-based fluorescent imaging agent for cancer. Biochemical and biophysical research communications 2009;390(3):624–9. [PubMed: 19818734]
30. Hoogstins CE, Tummers QR, Gaarenstroom KN, de Kroon CD, Trimbos JB, Bosse T, et al. A Novel Tumor-Specific Agent for Intraoperative Near-Infrared Fluorescence Imaging: A Translational Study in Healthy Volunteers and Patients with Ovarian Cancer. Clinical cancer research : an official journal of the American Association for Cancer Research 2016;22(12):2929–38. [PubMed: 27306792]
31. Proulx ST, Luciani P, Christiansen A, Karaman S, Blum KS, Rinderknecht M, et al. Use of a PEG-conjugated bright near-infrared dye for functional imaging of rerouting of tumor lymphatic drainage after sentinel lymph node metastasis. Biomaterials 2013;34(21):5128–37. [PubMed: 23566803]
32. Rosenthal EL, Warram JM, de Boer E, Chung TK, Korb ML, Brandwein-Gensler M, et al. Safety and Tumor Specificity of Cetuximab-IRDye800 for Surgical Navigation in Head and Neck Cancer. Clinical cancer research : an official journal of the American Association for Cancer Research 2015;21(16):3658–66. [PubMed: 25904751]
33. Lamberts LE, Koch M, de Jong JS, Adams ALL, Glatz J, Kranendonk MEG, et al. Tumor-Specific Uptake of Fluorescent Bevacizumab-IRDye800CW Microdosing in Patients with Primary Breast Cancer: A Phase I Feasibility Study. Clinical cancer research : an official journal of the American Association for Cancer Research 2017;23(11):2730–41. [PubMed: 28119364]
34. Zettlitz KA, Tsai WK, Knowles SM, Kobayashi N, Donahue TR, Reiter RE, et al. Dual-modality immunoPET and near-infrared fluorescence (NIRF) imaging of pancreatic cancer using an anti-prostate cancer stem cell antigen (PSCA) cys-diabody. J Nucl Med 2018 doi 10.2967/jnumed.117.207332.
35. Namikawa K, Tsutsumida A, Tanaka R, Kato J, Yamazaki N. Limitation of indocyanine green fluorescence in identifying sentinel lymph node prior to skin incision in cutaneous melanoma. International journal of clinical oncology 2014;19(1):198–203. [PubMed: 23371310]
36. Toh U, Iwakuma N, Mishima M, Okabe M, Nakagawa S, Akagi Y. Navigation surgery for intraoperative sentinel lymph node detection using Indocyanine green (ICG) fluorescence real-time

imaging in breast cancer. Breast cancer research and treatment 2015;153(2):337–44. [PubMed: 26267663]

37. Currie AC, Brigic A, Thomas-Gibson S, Suzuki N, Moorghen M, Jenkins JT, et al. A pilot study to assess near infrared laparoscopy with indocyanine green (ICG) for intraoperative sentinel lymph node mapping in early colon cancer. European journal of surgical oncology : the journal of the European Society of Surgical Oncology and the British Association of Surgical Oncology 2017;43(11):2044–51.
38. Buda A, Crivellaro C, Elisei F, Di Martino G, Guerra L, De Ponti E, et al. Impact of Indocyanine Green for Sentinel Lymph Node Mapping in Early Stage Endometrial and Cervical Cancer: Comparison with Conventional Radiotracer (99m)Tc and/or Blue Dye. Annals of surgical oncology 2016;23(7):2183–91. [PubMed: 26714944]
39. Cai QY, Yu P, Besch-Williford C, Smith CJ, Sieckman GL, Hoffman TJ, et al. Near-infrared fluorescence imaging of gastrin releasing peptide receptor targeting in prostate cancer lymph node metastases. The Prostate 2013;73(8):842–54. [PubMed: 23280511]
40. Schwarzenboeck SM, Rauscher I, Bluemel C, Fendler WP, Rowe SP, Pomper MG, et al. PSMA Ligands for PET Imaging of Prostate Cancer. J Nucl Med 2017;58(10):1545–52. [PubMed: 28687599]
41. Bahrenberg G, Brauers A, Joost HG, Jakse G. Reduced expression of PSCA, a member of the LY-6 family of cell surface antigens, in bladder, esophagus, and stomach tumors. Biochem Biophys Res Commun 2000;275(3):783–8. [PubMed: 10973799]

Translational Relevance

The completeness of radical prostatectomy is the cornerstone of successful treatment for localized prostate cancer. However, the inability to visualize tumor margins and metastases to regional lymph nodes intraoperatively increases the likelihood of positive margins, tumor recurrence, and possibly side effects from over-treatment. Here we report the development of a novel targeted fluorescence-imaging probe, A11 Mb-IRDye800CW, which recognizes a cell surface marker of prostate tumors and visualizes PSCA-positive disease with high sensitivity and specificity. A11 Mb-IRDye800CW was successfully used to detect primary tumor and lymph node metastases, and for fluorescent image-guided surgery to visualize tumor margins, facilitating more complete cytoreduction, and thereby improving overall survival. The clinical translation of such probes has the potential to improve the surgical outcome of patients with prostate cancer significantly.

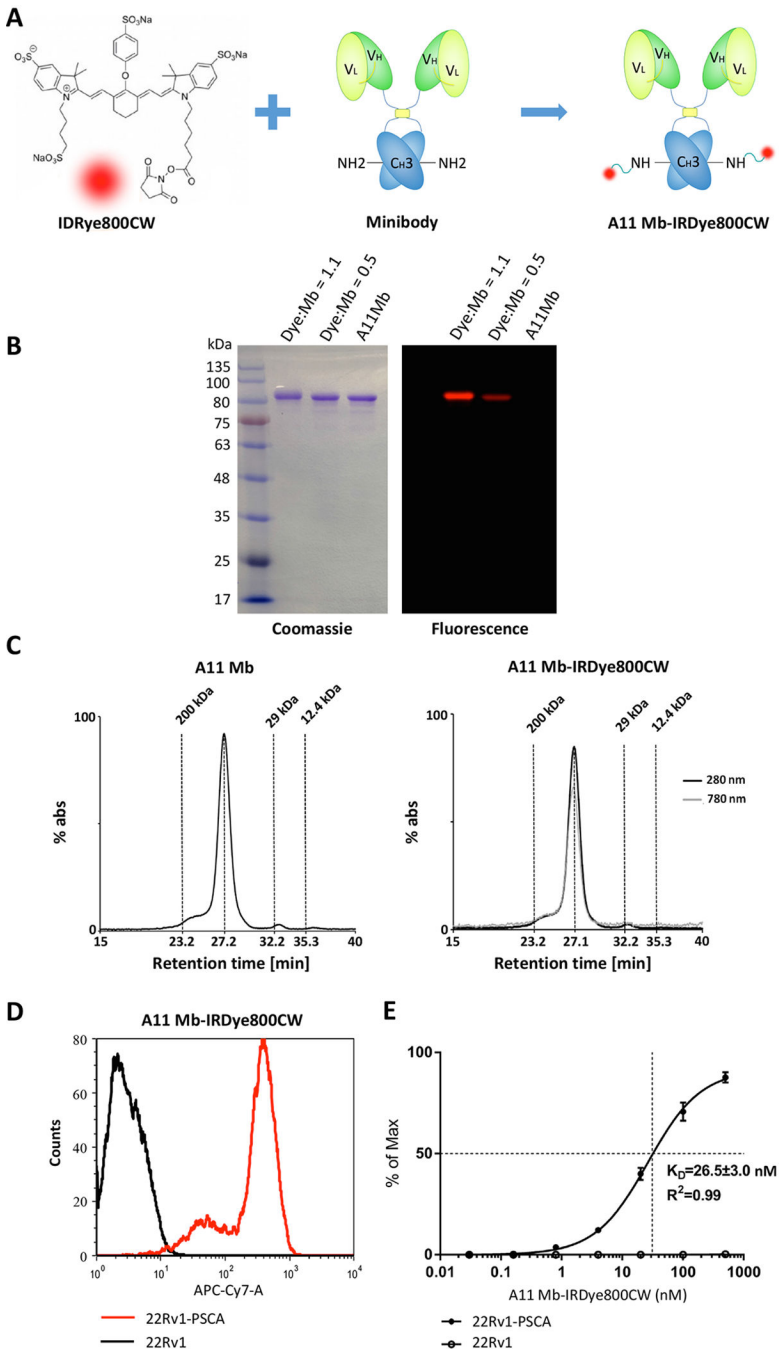

Figure 1.

Biochemical and functional characterization of IRDye800CW-conjugated anti-PSCA A11 Mb.

A, schematic of the conjugation of A11 Mb with IRDye800CW NHS ester (IRDye800CW). B, non-reducing SDS-PAGE demonstrated the conjugation of A11 Mb with IRDye800CW. Higher dye-to-protein ratio (1.1) yielded a stronger fluorescent band than the reaction at lower ratio (0.5) (Right). Minibody (80 kDa) was visualized by Coomassie blue stain (Left). C, size-exclusion chromatography of purified A11 Mb and A11 Mb-IRDye800CW. Elution

time of standard proteins is indicated. D, flow cytometry analysis of the A11 Mb-IRDye800CW binding to 22Rv1-PSCA cells and to 22Rv1 parental cells. E, quantitative flow cytometry showed specific binding of A11 Mb-IRDye800CW to 22Rv1-PSCA cells with an apparent affinity of 26.5 ± 3.0 nM.

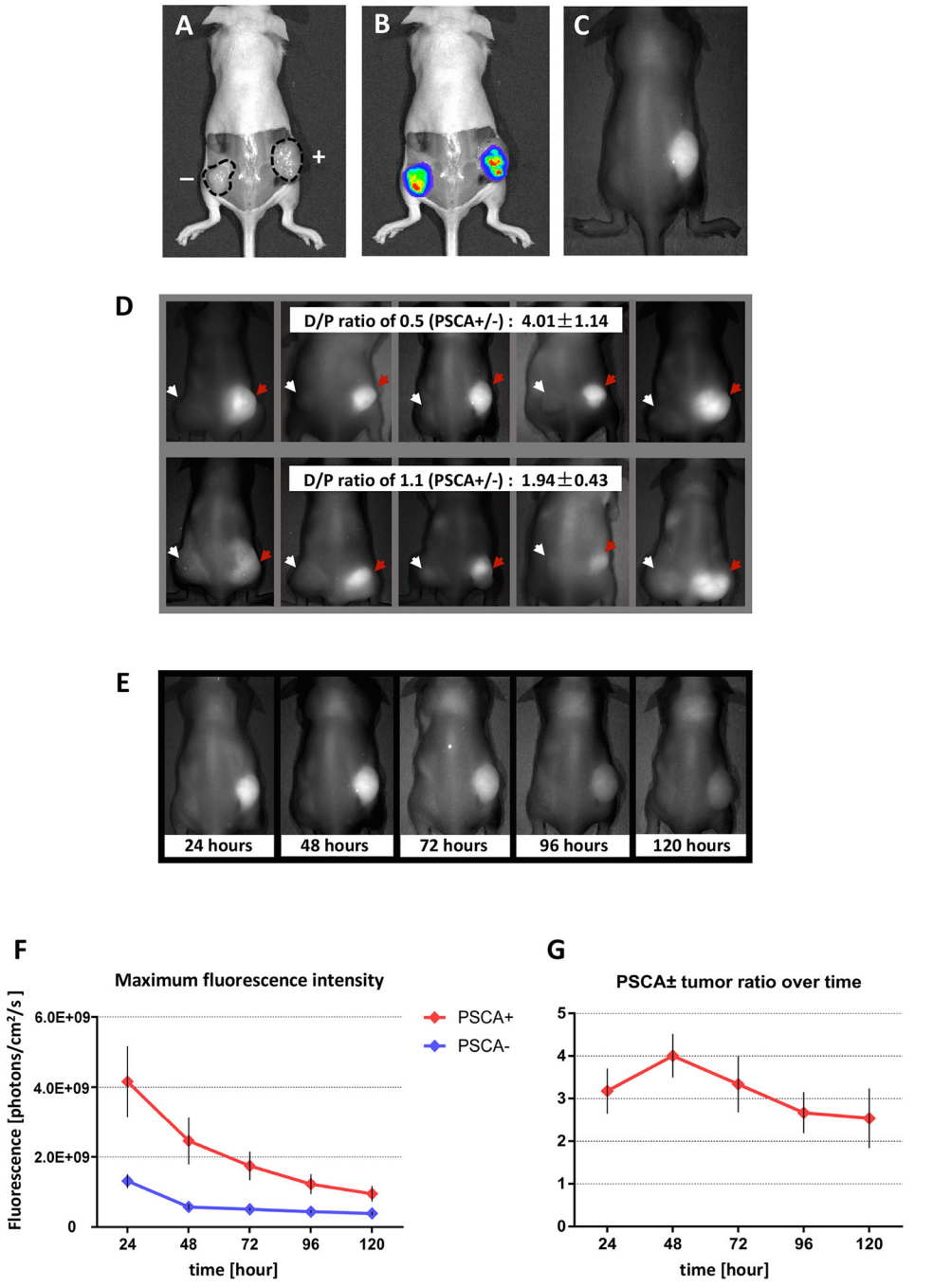

Figure 2.

Determination of the optimal imaging parameters for detection of PSCA expressing tumors *in vivo* using A11 Mb-IRDye800CW.

A-C, a representative mouse bearing 22Rv1-PSCA (right flank) and 22Rv1 (left flank). Tumors were imaged under white light (A), bioluminescence (B) and fluorescence (C). The contour of tumors is marked by the dashed line. Both 22Rv1-PSCA and 22Rv1 tumors showed bioluminescent signals due to luciferase expression. Fluorescent signals were detected by A11 Mb-IRDye800CW in the PSCA+ tumor. D, two different dye-to-protein

ratios of A11 Mb-IRDye800CW probe intravenously administrated to tumor-bearing mice (22Rv1-PSCA, right flank. PSCA-negative 22Rv1, left flank) (5 mice per group). Fluorescence images were captured 48 hours post-injection. Red arrow, PSCA+ tumor. white arrow, PSCA- tumor. Mean of PSCA +/− tumor signal ratios is indicated. E–G, five mice bearing 22Rv1-PSCA (right flank) and PSCA-negative 22Rv1 (left flank) tumors received 25 μg of A11 Mb-IRDye800CW (D/P ratio: 0.5) intravenously and imaged at time indicated after probe injection. E, serial images of a representative mouse over time. F, average maximum fluorescence intensity of PSCA+ and PSCA- tumors over time after probe injection. G, the average ratios of the maximum fluorescence intensities of PSCA+ tumor compared to the PSCA- tumor from each mouse over time.

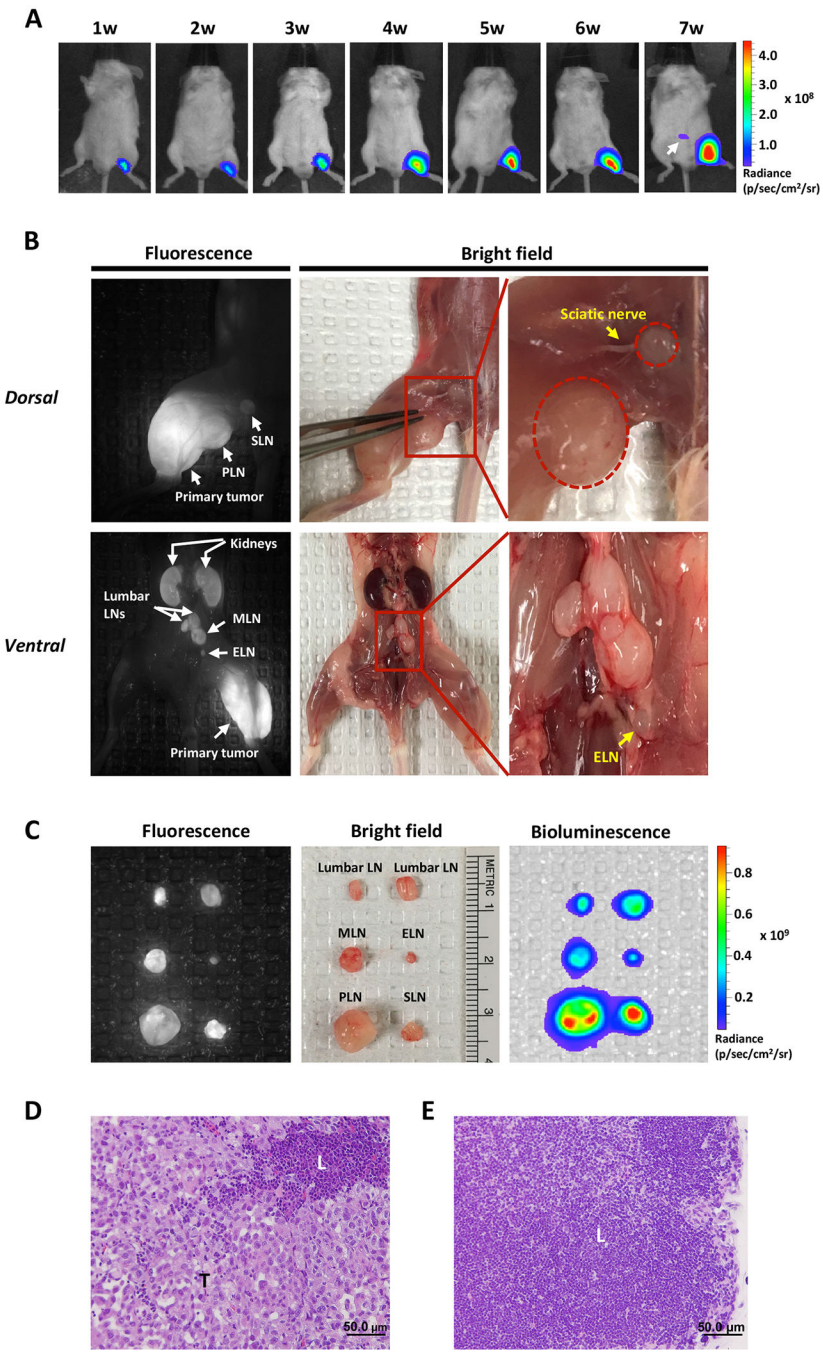

Figure 3.

Detection of tumor metastasis in lymph nodes by A11 Mb-IRDye800CW fluorescent imaging.

A, LN metastasis model was established by hock injection of PC3-PSCA-Fluc cells and the development of metastasis (white arrow) was monitored by BLI weekly. B, optical fluorescence images of multiple metastatic LNs with A11 Mb-IRDye800CW probe. In dorsal view, the primary tumor and enlarged sentinel LNs (popliteal and sciatic LN) were detected by fluorescence imaging. In ventral view, metastatic lumbar LNs, medial iliac LN,

and external iliac LN were detected by fluorescence imaging. C, *ex vivo* optical imaging by BLI, fluorescence and bright field. D and E, Histology of resected fluorescent LN (external iliac LN) showed tumor metastases (D). Normal lymph node (E). T, tumor tissue; L, lymphatic tissue. SLN, sciatic lymph node; PLN: popliteal lymph node; MLN: medial iliac lymph node, ELN: external iliac lymph node. Scale bar, 50μm.

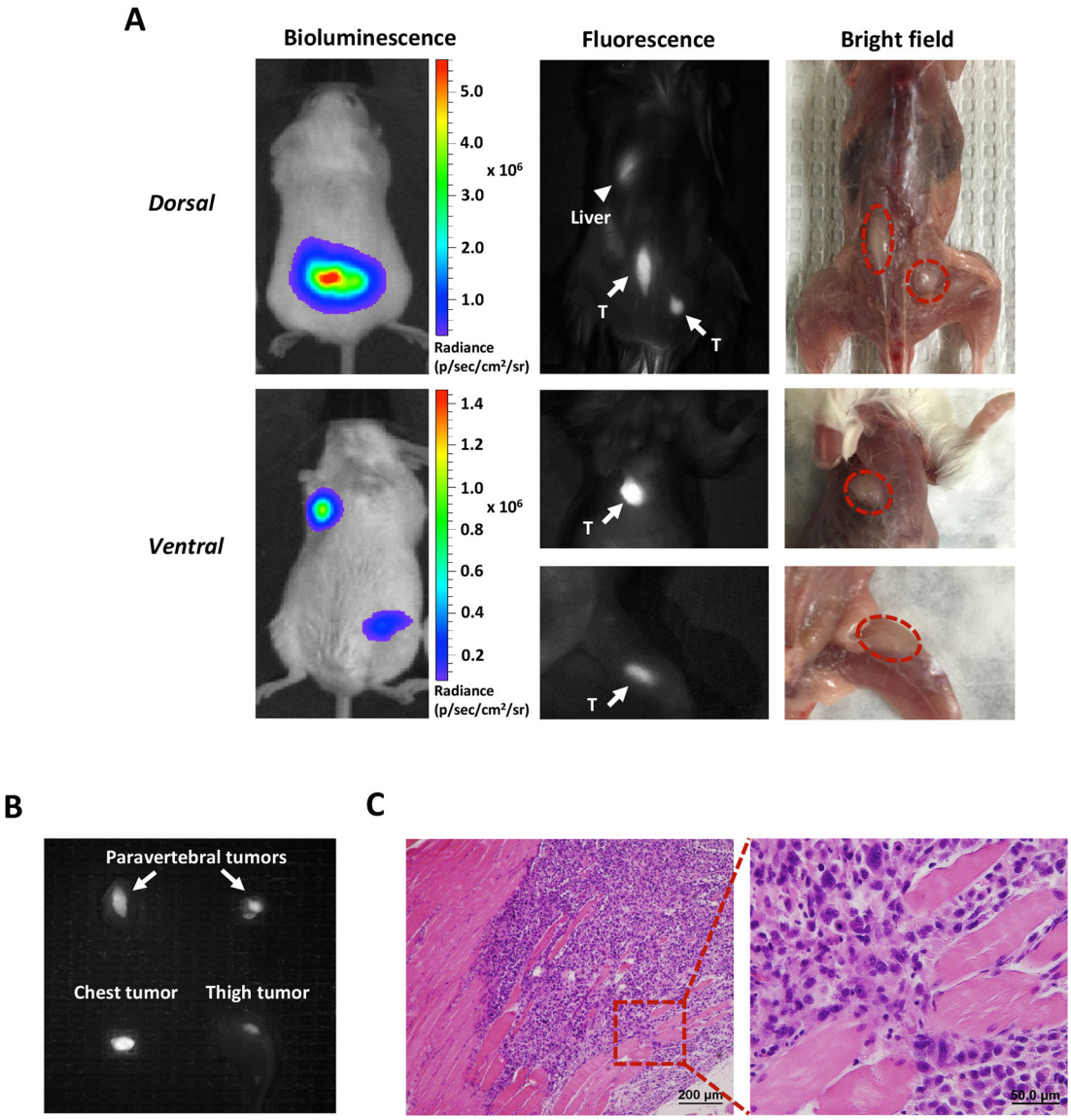

Figure 4.

Detection of PC3-PSCA-Fluc distant metastatic tumors by A11 Mb-IRDye800CW fluorescent imaging.

A, images of multiple distant metastases in SCID mice under the BLI, fluorescence and bright field. In dorsal view, fluorescence imaging identified the paravertebral tumors (arrows) that were detected by bioluminescence (marked by the red dotted lines in the bright field). Fluorescent signal in liver is due to clearance of minibody (arrowhead). In ventral view, the tumors located on the chest and the left thigh were detected by both bioluminescence and fluorescence imaging (arrows). B, *ex vivo* fluorescent images of metastatic tumors from A. C, H&E staining of the resected fluorescent tissue sample (thigh tumor) confirmed tumor cell infiltration. T, tumor.

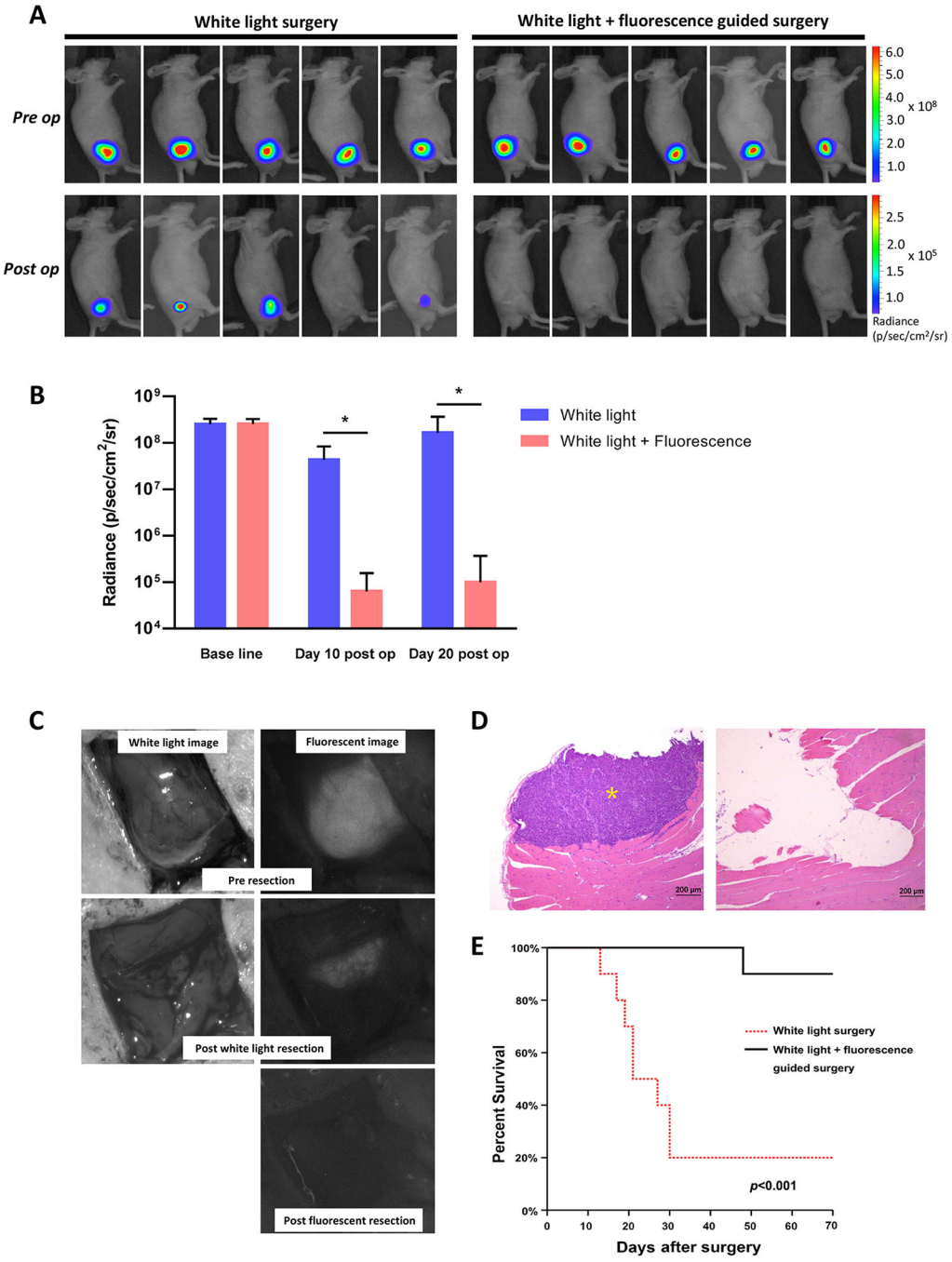

Figure 5.

A11 Mb-IRDye800CW fluorescent imaging enabled surgical resection of infiltrative 22Rv1-PSCA-Fluc tumors under fluorescence guidance in real-time. A, representative pre- and post-operative bioluminescence images: white light surgery only (n=10) and white light + fluorescence guided surgery (n=10). B, tumor resection under fluorescent guidance significantly decreased the tumor burden at days 10 and 20 post operation, compared with white light surgery alone. *, $p < 0.001$. C, intraoperative images of tumors under white light and fluorescence before and after tumor resection surgery. D, H&E histology of surgical

margins showing residual tumor tissue after white light surgery (left) and negative surgical margin after secondary fluorescence-guided surgery (right). Yellow asterisk, tumor cells. E, Kaplan-Meier analysis showing a significant difference in survival of the fluorescence-guided surgery group (n=10) and the mice which received conventional white light surgery (n=10) (log rank $p< 0.001$).

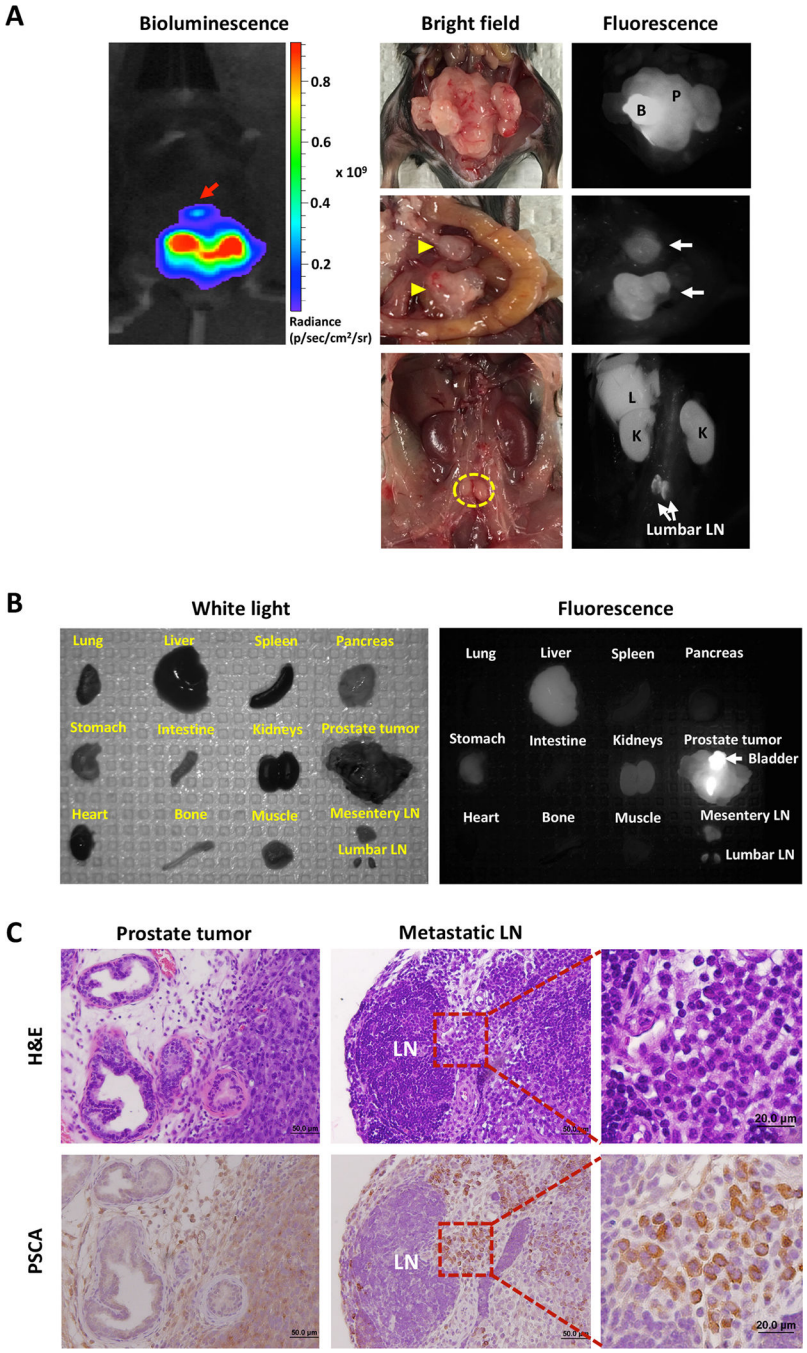

Figure 6.

Optical imaging with A11 Mb-IRDye800CW enabled detection of orthotopically implanted intraprostatic tumors and metastatic lesions in human PSCA knock-in transgenic mice. A, bioluminescence image of the prostate tumor and metastasis (red arrow) (left top panel). Optical images of the orthotopic tumor, mesentery (yellow arrowhead) and lumbar LNs (yellow dotted line) metastases under bright field and fluorescence. Fluorescence imaging with A11 Mb-IRDye800CW detected the orthotopic tumor and multiple LNs metastases. Nonspecific fluorescent signals in the liver and kidneys are due to the clearance of probe. B,

ex vivo optical imaging for evaluation of probe biodistribution in transgenic mouse. C, H&E and IHC staining for human PSCA confirmed the presence of tumor cells and PSCA expression in the prostate and metastatic lumbar LNs. B, bladder; P, prostate tumor; L, liver; K, kidney; LN, lymph node.